A Theoretical Study of the UV/Visible Absorption and Emission Solvatochromic Properties of Solvent-Sensitive Dyes

Wen-Ge Han,*[a] Tiqing Liu,[a, c] Fahmi Himo,[a, d] Alexei Toutchkine,[b] Donald Bashford,[a, e] Klaus M. Hahn,[b] and Louis Noodleman*[a]

Using the density-functional vertical self-consistent reaction field (VSCRF) solvation model, incorporated with the conductor-like screening model (COSMO) and the self-consistent reaction field (SCRF) methods, we have studied the solvatochromic shifts of both the absorption and emission bands of four solvent-sensitive dyes in different solutions. The dye molecules studied here are: S-TBA merocyanine, Abdel-Halim's merocyanine, the rigidified amino-coumarin C153, and Nile red. These dyes were selected because they exemplify different structural features likely to impact the solvent-sensitive fluorescence of "push-pull", or merocyanine, fluorophores. All trends of the blue or red shifts were correctly predicted, comparing with the experimental observations. Explicit H-bonding interactions were also considered in several protic solutions like H_2O, methanol and ethanol, showing that including explicit H-bonding solvent molecule(s) in the calculations is important to obtain the correct order of the excitation and emission energies. The geometries, electronic structures, dipole moments, and intra- and intermolecular charge transfers of the dyes in different solvents are also discussed.

1. Introduction

Since solvent-solute interactions can change the geometry, the electronic structure, and the dipole moment of a solute, UV/Vis absorption or/and emission (fluorescence) band positions of solvent-sensitive dyes will vary with the polarity of the medium. This phenomena is called solvatochromism.[1] According to the Franck–Condon principle,[2] optical absorption is a vertical excitation process, in which the electronic distribution in both the solute and solvent is altered, while the nuclear coordinates of the solute, as well as the solvent molecules are unchanged. In liquid solutions, the solute and solvent molecules will normally reorient after excitation, and a new solvation equilibrium in the excited state will be established. Then emission or fluorescence will happen from this equilibrium state. Again, this is also a vertical electronic transition process.

If the solute has an appreciable dipole and no net charge, the ground (or relaxed excited) state solvation results largely from the dipole–dipole interactions between the solvent and the solute; there is an oriented solvent cage around the dipolar solute, leading to a net stabilization between the ground (or relaxed excited) state solute and the solvent molecules.[1] Normally, if the solute dipole moment in the excited state is larger than that in the ground state, the excited state is better stabilized relative to the ground state. With increasing solvent polarity, there will be a red shift for both the absorption and emission bands. On the other hand, a blue shift will occur if the solute dipole moment in the ground state is larger than that in the excited state.

Very recently, we established a density-functional vertical self-consistent reaction field (VSCRF) solvation model for predicting vertical excitation energies and the solvatochromic shift of solvent-sensitive dyes in different solutions.[3] Similar methods have been used to analyze the influence of surrounding protein residues and solvent on the optical absorption of the chromophore of photoactive yellow protein.[4] This VSCRF model was developed in the framework of density functional theory with ΔSCF methodology. Its implementation is based on our original self-consistent reaction field (SCRF) development,[5–8] where the solute molecule is computed by density functional theory in the presence of a solvent reaction field. The reaction field is

[a] Dr. W.-G. Han, Prof. L. Noodleman, Dr. T. Liu, Dr. F. Himo, Prof. D. Bashford
Department of Molecular Biology, TPC-15, The Scripps Research Institute
10550 North Torrey Pines Road, La Jolla, California 92037 (USA)
Fax: (+1) 858-784-8896
E-mail: wengehan@scripps.edu, lou@scripps.edu

[b] Dr. A. Toutchkine, Prof. K. M. Hahn
Department of Cell Biology, CB 164, The Scripps Research Institute
10550 North Torrey Pines Road, La Jolla, California 92037 (USA)

[c] Dr. T. Liu
Current address:
Department of Chemistry and Biochemistry
Montana State University
Bozeman, Montana 59717 (USA)

[d] Dr. F. Himo
Current address:
Royal Institute of Technology, SCFAB, Department of Biotechnology
Theoretical Chemistry, 106 91 Stockholm (Sweden)

[e] Prof. D. Bashford
Current address:
Hartwell Center
St. Jude Children's Research Hospital
332 N. Lauderdale St., Memphis TN 38105 (USA)

Supporting information for this article is available on the WWW under http://www.chemphyschem.org or from the author.

  DOI: 10.1002/cphc.200300801

evaluated from a finite-difference solution to the Poisson–Boltzmann equation and self-consistency between the reaction field and the electronic structure of the solute is achieved by iteration. In SCRF calculations, the nuclei and electrons of both the solute and solvent are relaxed. Once the SCRF of the S_0 state (or S_1 state) is determined, the VSCRF procedure on the S_1 state (or S_0 state) only allows the reorganization of the electronic structures of both the solute and solvent, and the vertical excitation (or emission) in solution is then obtained.

In another paper,[3] these methods were applied to predict the UV absorption blue shift of Brooker's merocyanine in $CHCl_3$ and H_2O solutions. The importance of relaxation of the molecular structures and of including the explicit H-bonding H_2O molecules is also discussed there. Herein, we will present applications to the molecules S-TBA merocyanine,[9] Abdel-Halim's merocyanine,[10] the rigidified aminocoumarin with a julolidine structure (C153),[1, 11–15] and Nile red,[16, 17] predicting the solvatochromic shift of both the absorption and emission processes. The importance of H-bonding effects on dye properties will also be discussed. These new structures test the applicability of our approach to molecules which can be useful for studying protein conformational changes in living cells.[18] This work can ultimately lead to design of practical solvent-sensitive fluorophores for live cell studies.

2. Methodology

The details of the VSCRF method are given in ref. [3]. Here we just briefly describe the theoretical framework and calculational steps to obtain the vertical excitation and emission energies of the solute in different solvents.

All quantum mechanical DFT calculations were performed using the Amsterdam Density Functional (ADF, Version 2000) package.[19, 20] The parametrization of Vosko, Wilk and Nusair (VWN)[21] was used for the local density approximation term, and the corrections of Becke(1988) (B)[22] and Perdew(1986) (P)[23] were used for the nonlocal exchange and correlation terms. The molecular orbitals were expanded in an uncontracted triple-ζ Slater-type orbital basis set, along with a single set of polarization functions, which constitutes basis set IV in the ADF code. The inner core shells of C(1s), N(1s), O(1s) and S(1s,2p) were treated by the frozen core approximation. The accuracy parameter (accint) for the numerical integration grid was set to 4.0.

Since the solute geometry varies with the solvent, we needed to obtain the optimized geometries of the solute in different solvents with different polarities. When studying the absorption blue shift of Brooker's merocyanine, we saw that relaxing the molecular structures in $CHCl_3$ and H_2O solutions was important in improving the relative excitation energy. Here again we used the COSMO (conductor-like screening model) in ADF to geometry optimize the solute structure in different solvent media.[24–26] The COSMO model is a dielectric solvent continuum model in which the solute molecule is embedded in a molecular-shaped cavity surrounded by a dielectric medium with given dielectric constant ε. For absorption processes, the ground state (S_0) of the solute was relaxed in different solvent dielectrics. For the emission processes, geometry optimizations were performed on the first excited singlet state (S_1). An electron was promoted from β-HOMO to β-LUMO during the S_1-state geometry optimizations.

The next step was to perform SCRF[5–8] calculations on the optimized (S_0 or S_1 state) geometries, in order to obtain the reaction field potential for VSCRF calculations. The solute molecule with the COSMO-optimized structure was again computed by VWN–BP method in the presence of a solvent reaction field (with dielectric constant ε).

The SCRF procedure is described briefly as follows. 1) One performs a gas-phase single-point energy calculation on the COSMO-optimized (S_0 or S_1 state) solute structure. 2) The CHELPG program[5] is then used to fit the point charges of each atom from the molecular electrostatic potentials (ESP) calculated by ADF. 3) One performs the solvation calculation by using the MEAD (Macroscopic Electrostatics with Atomic Detail) program developed by Bashford,[27–30] to solve the Poisson–Boltzmann equation with a numerical finite-difference method. 4) One adds the reaction field potential obtained from step 3) to the Hamiltonian of the ADF single-point energy calculation. The iteration of 1)–4) continues until self-consistency between the reaction field potential and the electronic structure of solute is achieved.

For the emission process, we also performed the first excited triplet state (T_1) SCRF calculation (promoting an electron from β-HOMO to α-LUMO) at the S_1 state COSMO-optimized geometries, since the S_1 state energy (E_{S1}') in the ΔSCF calculation has to be corrected because of spin-contamination.[31, 32] With the energy obtained from the T_1 state calculation designated as E_{T1}, the S_1 state energy after spin-decontamination will be [Equation (1)]:[31, 32]

$$E_{S1} = 2E_{S1}' - E_{T1} \quad (1)$$

In COSMO, charge fit and MEAD calculations, the van der Waals radii for atoms S, C, O, N, and H were taken as 1.8, 1.67, 1.4, 1.55, and 1.2 Å, respectively. The dielectric constants of the solvents we used in COSMO and MEAD (in SCRF) calculations were $\varepsilon = 80.0$ for H_2O, $\varepsilon = 37.5$ for acetonitrile, $\varepsilon = 36.7$ for dimethylformamide (DMF), $\varepsilon = 32.6$ for methanol (MeOH), $\varepsilon = 24.3$ for ethanol, $\varepsilon = 20.7$ for acetone, $\varepsilon = 10.2$ for 1,2-dichloroethane ($C_2H_4Cl_2$), $\varepsilon = 6.0$ for ethyl acetate, $\varepsilon = 2.3$ for benzene (C_6H_6), and $\varepsilon = 2.0$ for cyclohexane. The dielectric boundary between the interior (with $\varepsilon = 1$) and the exterior of the solute region was defined by the contact surface of rolling a probe sphere (with radius $r = 1.4$, 3.2, 3.7, 2.5, 3.0, 3.4, 4.0, 4.2, 3.5, and 3.3 Å, for the above solutions, respectively) over the solute in both COSMO and MEAD calculations.

After the SCRF was converged, the electronic density distribution and the potential resulting from the reaction field, and the ESP charges at the nuclei were then saved for VSCRF calculation. According to the VSCRF principle,[3] the absorption (E_{abs}) or emission (E_{em}) energy can be described as [Equation (2)]:

$$E_{abs}\ (\text{or } -E_{em}) = \Delta G^{if} = E_0{}^f - E_0{}^i + {}^1/_2\{\int [2\phi_i(x) + \Delta\phi_{op}(x)]\Delta\rho_{if}(x)d^3x\} = \Delta E_0 + \Delta G_{pot} + \Delta G_{res} \quad (2)$$

where $E_0{}^i$ and $E_0{}^f$ are the solute electronic energies of the initial and final charge distributions, respectively; ϕ_i is the reaction potential of ρ_i (from the initial electronic density and nuclear charge distribution) obtained from Poisson solutions for the initial state with the solvent dielectric ε (e.g. $\varepsilon = 80.0$ for water) outside the cavity. During the vertical electronic transition, the dielectric constant $\varepsilon_{op} = 2.0$ is set to the solvent region, which corresponds to the relaxation of the solvent electronic distribution. And $\Delta\phi_{op}$ is the reaction potential of $\Delta\rho_{if}$ obtained from Poisson solutions with the outside dielectric set to ε_{op}. The vertical transition energy is described by the sum of three terms: 1) $\Delta E_0 = E_0{}^f - E_0{}^i$ is the change in solute electronic energy upon excitation or emission; 2) the potential term [Equation (3)]

$$\Delta G_{pot} = \int \phi_i(x)\Delta\rho_{if}(x)d^3x \quad (3)$$

which describes the change of the reaction field energy caused by the reorganization of the solute electronic structure; and 3) the response term [Equation (4)]

$$\Delta G_{res} = {}^1/_2\{\int \Delta\phi_{op}(x)\Delta\rho_{if}(x)d^3x\} \quad (4)$$

which is the change of the free energy due to the electronic relaxation in solvent.

The iterative procedure in VSCRF can be described as follows: 1) For an absorption process, both the S_1 and T_1 state single-point energy calculations were performed at the S_0 state COSMO-optimized geometry. The reaction field potential (ϕ_i) of the solvated relaxed S_0 state (obtained from converged SCRF) was added to the Hamiltonian of the two S_1 and T_1 state calculations. For the emission process, two S_0 state single-point energy calculations were performed at the S_1 state COSMO-optimized geometry, and the reaction field potentials (ϕ_i) obtained from the S_1 and T_1 state SCRF calculations were added separately to the S_0 state calculations. 2) The electronic density distribution plus the charges of the nuclei (ρ_f) was taken from step 1), and the ESP charges were fitted. 3) The differences of electronic densities ($\Delta\rho_{if}$) between the current excited state (for absorption) or ground state (for emission) and the relaxed ground state (for absorption) or excited state (for emission) over the grids of ADF were computed. 4) A set of the ESP charge differences for each atom center between the current state and the relaxed state was also calculated. Using this set of ESP difference charges (again with $\varepsilon = 1$ in solute region), we then performed a MEAD calculation to get the reaction field potential ($\Delta\phi_{op} = \Delta\phi_{if}$) corresponding to the electronic relaxation of the solvent ($\varepsilon_{op} = 2$ in the solvent region). Then the vertical absorption or emission energy was computed from Equation (2).[3] 5) $\phi_i + \Delta\phi_{if}$ was then added back to the Hamiltonian of ADF calculation in step 1). The iteration of steps 1)–5) was repeated until self-consistency between the electron relaxation in solute and in solvent was achieved. Note that for any S_1 state energy, spin-decontamination had to be applied according to Equation (1).

3. Results and Discussion

The methodology mentioned above was applied to the dye molecules S-TBA merocyanine, Abdel-Halim's merocyanine, rigid aminocoumarin C153, and Nile red, to predict the solvatochromic properties for both absorption and emission. Their S_0 and S_1 state geometries, electronic distributions and dipole moment properties were also studied. The four molecules have different π electronic structures. The first two are merocyanine dyes with extended central C—C bonds. One can expect that, as we found for Brooker's merocyanine,[3] both their electronic and molecular structures (especially along the central C—C bonds), and their dipole moments in S_0 and in S_1 state, will vary in different solvents with different polarities. In contrast, the aminocoumarin C153 and Nile red are relatively rigid, but we will see from the calculations that their structures and dipole moments also change upon solvation in different solvents.

3.1. S-TBA Merocyanine

The S-TBA dyes (with different side chains connected to the nitrogen atoms) have been used to make biosensors reporting calcium and calmodulin binding in living cells.[9, 18, 33] A blue shift occurs for this dye in both the absorption (17 nm) and emission (14 nm) bands with increasing solvent polarity from C_6H_6 to MeOH solutions. The structure of the S-TBA merocyanine we calculated is shown in Figure 1. In Table 1, we present the predicted and experimentally observed vertical excitation (E_{abs}) and emission (E_{em}) energies, and the calculated dipole moment values for the relaxed S_0 state, the Franck–Condon S_1 state, the

Table 1. SCRF/VSCRF calculated and experimentally observed absorption (E_{abs}) and emission (E_{em}) energies (eV), and the relaxed S_0 (μ_{S0}) and S_1 (μ_{S1}) state dipole moment values (D) for S-TBA merocyanine in different environments.

	Absorption				Emission			
			E_{abs}				E_{em}	
Solvent	μ_{S0}[a]	μ^v_{S1}[b]	Calculation	Experiment	μ_{S1}[c]	μ^v_{S0}[d]	Calculation	Experiment
Gas phase	13.15	13.13	1.627		13.34	14.42	1.488	
C_6H_6	17.72	19.05	1.570	2.067	18.41	18.10	1.486	2.010
MeOH	24.84	21.29	1.625	2.127	21.40	22.41	1.491	2.046

[a] Dipole moment of the relaxed S_0 state. [b] Dipole moment for the vertical excited Franck–Condon S_1 state. [c] For the relaxed S_1 state. [d] For the Franck–Condon S_0 state in the vertical emission process.

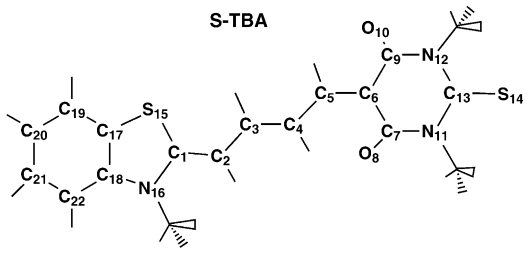

Figure 1. Structure and atomic labeling for S-TBA merocyanine.

relaxed S_1 state, and the Franck – Condon S_0 state of the S-TBA in the gas phase, and in C_6H_6 and MeOH solutions.

It has been found and also appears here that the ΔSCF procedure of DFT method underestimates the absolute value of the S_1 state energy.[3, 34] The possible reason is that the ground-state orbitals may not be strictly orthogonal to the excited state orbitals in the ΔSCF calculations. Some error of the under-estimation may also caused by the fact that, the solute molecules are not strictly planar while interacting explicitly with the solvent molecules.[34] However, we will focus here on the relative excitation and emission energies to predict the solvent dependency. From C_6H_6 to MeOH solutions (see Table 1), the observed blue shift character for both the absorption and emission is correctly predicted by the SCRF/VSCRF calculations at the COSMO-optimized geometries. While the predicted relative emission energy, $E_{em}(\text{MeOH}) - E_{em}(C_6H_6)$ (0.005 eV), is smaller than the observed value of 0.036 eV, our prediction of the excitation energy shift for $E_{abs}(\text{MeOH}) - E_{abs}(C_6H_6)$ is (0.055 eV), very close to the experimental value (0.060 eV).

We have calculated that gas-phase S-TBA has the largest calculated $\pi \rightarrow \pi^*$ excitation energy, and there is a predicted red shift from the gas phase to C_6H_6 for absorption. The corresponding predicted red shift in emission is very small. We checked the electronic structure of S-TBA in the gas phase, and found that the HOMO of the S_0 state was occupied mainly (78.1 %) by the in-plane *n* orbital of atom S_{14} (see Figure 2, S_0(HOMO-*n*) in the gas phase). The orbital below the HOMO is then occupied by the out-of-plane π orbitals of the atoms C_6(16.1 %), C_2(14.6 %), C_4(14.4 %), S_{14}(10.7 %), S_{15}(7.6 %), and N_{16}(7.2 %). The energy difference of these two orbitals in the DFT ground state is 1.205 eV. Our ΔSCF S_1 state calculation, however, predicted a $\pi \rightarrow \pi^*$ transition (see Figure 2, S_1(π-hole), and S_1(SOMO-π*)) for the hole and the promoted electron molecular orbital in the S_1 state). SOMO is a singly occupied molecular orbital in the excited state. Presumably at the ΔSCF level, the $n \rightarrow \pi^*$ is higher in energy than the $\pi \rightarrow \pi^*$ transition for the gas-phase S-TBA. It is not true for the time-dependent DFT (TDDFT) calculation. The gas-phase TDDFT calculation for this structure showed that the excitation energy of the $n \rightarrow \pi^*$ transition (1.467 eV) is lower than the $\pi \rightarrow \pi^*$ transition (2.377 eV). However, the oscillator strength of the $n \rightarrow \pi^*$ process is almost zero (1.49×10^{-5}), while the $\pi \rightarrow \pi^*$ transition has the largest oscillator strength (0.90) among all the possible transitions. The excitation in the gas-phase TDDFT calculation is therefore also predicted to be a $\pi \rightarrow \pi^*$ transition with high excitation energy. In C_6H_6, the π orbital changes to be the HOMO in the ground state, which lies only 0.011 eV higher than the *n* orbital. In MeOH, the HOMO of the S_0 state is also occupied by the π orbital (see Figure 2, S_0(HOMO) in MeOH), and is 0.285 eV higher than the *n* orbital. The $S_0 \rightarrow S_1$ electronic excitations of the S-TBA in C_6H_6 and MeOH solutions are clearly $\pi \rightarrow \pi^*$ transitions. During the $\pi \rightarrow \pi^*$ process, the solute dipole moment increases in C_6H_6 and decreases in MeOH, which is consistent with the red shift of the absorption band from gas phase to C_6H_6 solution, and blue shift from C_6H_6 to MeOH. On the other hand, during the $\pi^* \rightarrow \pi$ emission, the solute dipole moment decreases in C_6H_6 and increases in MeOH, which is also in agreement with the predicted and the observed blue shift of the fluorescence spectra from C_6H_6 to MeOH.

The molecular structure of the solute should vary with its electronic structure. In Table 2, we present the main bond lengths of the S_0 and S_1 state S-TBA in gas phase, in C_6H_6 and MeOH solutions. In gas phase, the central C_1–C_2, C_2–C_3, C_3–C_4, C_4–C_5, and C_5–C_6 bonds in S_0 state are of double, single, double, single, and double bond characters. By contrast, in C_6H_6, these bond lengths are very close to each other, and then they reverse to single, double, single, double, and single bond characters in MeOH. The C_{13}–S_{14} bond length increases with increasing solvent polarity from 1.676 Å in gas phase to 1.695 Å in MeOH. In the relaxed S_1 state, the C–C bonds mentioned above changed to single, double, single, double, and single bond characters in the gas phase. In the nonpolar solution of C_6H_6, the bond lengths are also similar to each other, but C_2–C_3 and C_4–C_5

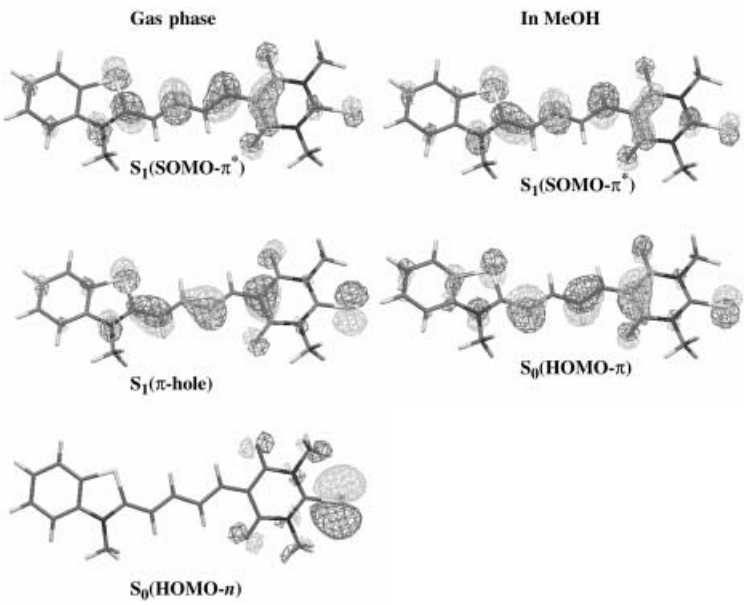

Figure 2. S-TBA merocyanine in gas phase and in MeOH solution. Molecular orbital plots for the electron in HOMO of the ground state (S_0) and the $\pi \rightarrow \pi^*$ promoted electron in the first excited singlet state (S_1). In the gas phase, the HOMO is an n *orbital, but the hole in the S_1 state is a π orbital. The figure is generated with MOLEKEL.[37]*

Table 2. *Main bond lengths (Å) of the S_0 and S_1 state S-TBA merocyanine geometries in gas phase and in C_6H_6 and MeOH solutions.*

	S_0 state			S_1 state		
Bond Length	Gas Phase	In C_6H_6	In MeOH	Gas Phase	In C_6H_6	In MeOH
C_1–C_2	1.394	1.395	1.418	1.414	1.412	1.394
C_2–C_3	1.408	1.400	1.386	1.395	1.401	1.413
C_3–C_4	1.386	1.392	1.410	1.420	1.415	1.399
C_4–C_5	1.407	1.398	1.388	1.388	1.396	1.407
C_5–C_6	1.390	1.402	1.416	1.422	1.418	1.414
C_{13}–S_{14}	1.676	1.687	1.695	1.686	1.689	1.699

are still a little shorter than C_1–C_2, C_3–C_4, and C_5–C_6. While in the polar solution of MeOH, the bond order reversed with C_2–C_3 and C_4–C_5 longer than C_1–C_2 and C_3–C_4. Clearly, for both the S_0 and S_1 states, the S-TBA changes from mainly one resonance structure in the gas phase to mainly another in MeOH. The geometry in C_6H_6 is a nearly equal mixture of these two resonance structures. It is, therefore, important to get the correct geometry of the solute in a specific solvent when studying the properties of the solute in solutions.[3, 35]

3.2. Abdel-Halim's Merocyanine

The next merocyanine (see any structure in Figure 3) was first synthesized by S. T. Abdel-Halim.[10] It is structurally similar to Brooker's merocyanine[3] but with a different position of the N–CH_3 group. Unlike Brooker's merocyanine,[1] which shows very weak emission, Abdel-Halim's merocyanine exhibits significant fluorescence.[10, 36]

In Table 3, we present the calculated dipole moment values and the predicted and experimentally observed vertical excitation (E_{abs}) and emission (E_{em}) energies of this dye molecule in different solvents.

With increasing solvent polarity, a blue shift was observed for both the absorption and emission bands for the Abdel-Halim's merocyanine. In our SCRF/VSCRF calculations at the COSMO-optimized geometries, we correctly predicted the relative band positions except for the absorption bands in acetonitrile and in MeOH. Since the dielectric constant of acetonitrile ($\varepsilon = 37.5$) is larger than that of MeOH ($\varepsilon = 32.6$), the predicted excitation energy of the solute molecule in acetonitrile is larger than that in MeOH, which is inconsistent

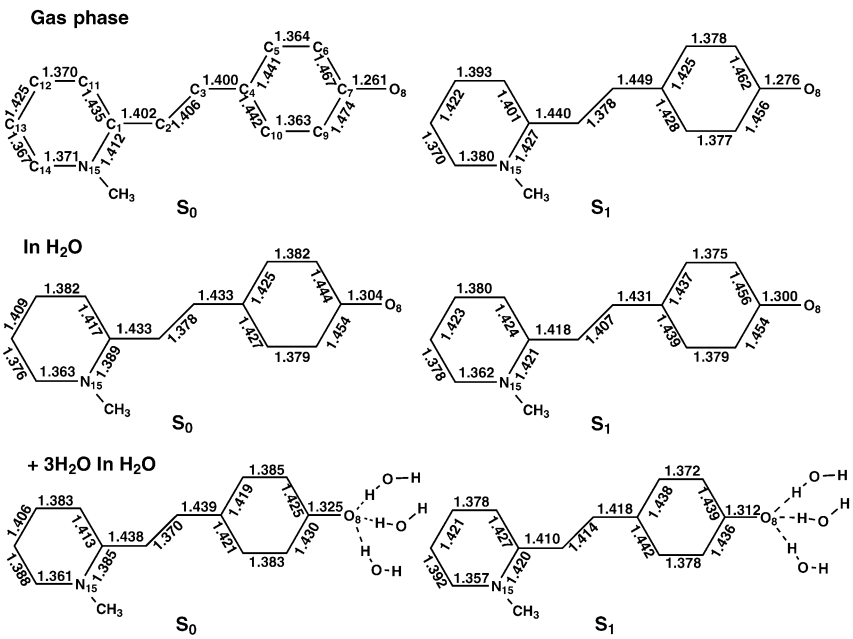

Figure 3. The main bond lengths of the Abdel-Halim's merocyanine in gas phase and in H_2O (without and with explicit H-bonding H_2O molecules) solution for both the relaxed S_0 and S_1 state.

Table 3. *SCRF/VSCRF calculated and experimentally observed absorption (E_{abs}) and emission (E_{em}) energies (eV), and the S_0 (μ_{S0}) and S_1 (μ_{S1}) state dipole moment values (D) for Abdel-Halim's merocyanine in different solvents.*

	Absorption				Emission			
			E_{abs}				E_{em}	
Solvent	μ_{S0}[a]	μ^v_{S1}[b]	Calculation	Experiment	μ_{S1}[c]	μ^v_{S0}[d]	Calculation	Experiment
Gas phase	13.48	12.06	1.660		11.08	14.54	1.365	
$C_2H_4Cl_2$	26.57	22.71	1.822	2.246	19.88	23.24	1.635	2.149
Acetone	28.64	24.48	1.906	2.263	20.81	24.23	1.656	2.168
Acetonitrile	29.41	25.21	1.945	2.357	21.28	24.73	1.671	2.214
MeOH no H-bonding	29.01	25.01	1.937	2.644	21.27	24.71	1.675	2.326
MeOH + $2CH_3OH$	30.42	25.73	2.067		22.09	25.48	1.731	
H_2O no H-bonding	30.36	26.16	1.999	2.911	22.06	25.40	1.690	2.408
H_2O + $3H_2O$	31.36	26.71	2.194		22.62	25.89	1.783	

[a] – [d] See footnotes under Table 1.

with the experiments. Though the predicted emission energy in MeOH is larger than that in acetonitrile, the energy difference is too small (0.004 eV), compared with the experimental value of 0.112 eV. Thinking that H-bonding interactions between atom O_8 of the solute and MeOH (CH_3OH) could further polarize the solute molecule and produce larger excitation and emission energies in MeOH than in acetonitrile, we next added two explicit CH_3OH molecules. These were in the same plane of the dye molecule, and H-bonded to the atom O_8 (see Figure 4a). Again the geometry was optimized using the COSMO solvation model. It turned out that, compared to the calculations without explicit CH_3OH molecules, both the excitation and emission energies were increased (by 0.130 and 0.056 eV, respectively) and the energy differences of $E_{abs}(+2CH_3OH) - E_{abs}$(acetonitrile) and $E_{em}(+2CH_3OH) - E_{em}$(acetonitrile) were much closer to the experimental data.

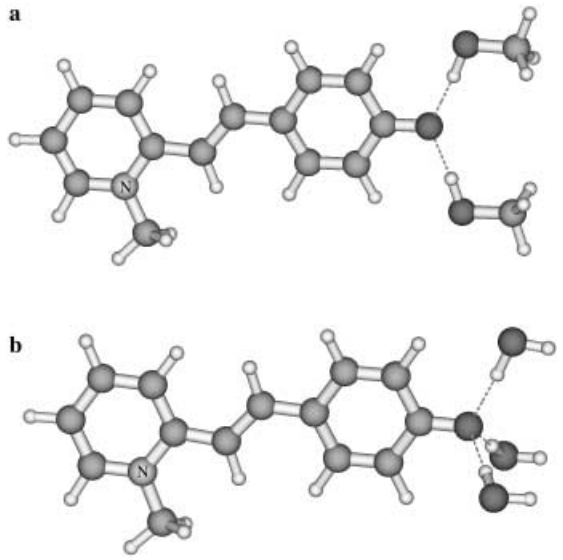

Figure 4. The H-bonding patterns of the two explicit CH_3OH and three H_2O molecules in a) $+2CH_3OH$ and b) $+3H_2O$ models for the Abdel-Halim's merocyanine in MeOH and in water, respectively. The figure is generated with XMOL[38] and XFIG.[39]

Even without considering explicit H-bonding interactions, the $E_{abs}(H_2O)$ and $E_{em}(H_2O)$ were predicted to be the largest among the values obtained in different solutions, which is in agreement with the experiments. However, the relative energies between $E_{abs}(H_2O)$ [or $E_{em}(H_2O)$] and the excitation (or emission) energies in other solutions were much smaller than the corresponding experimental values. When studying Brooker's merocyanine, we found there would be two to four water molecules H-bonding to the oxygen atom, which is a strong electron acceptor. Here we added three H_2O molecules around atom O_8, in a tetrahedral arrangement like a C-H_3 group (see Figure 4b). Now the predicted excitation energy changed from $E_{abs}(H_2O) = 1.999$ eV to $E_{abs}(+3H_2O) = 2.194$ eV, and the emission energy increased from $E_{em}(H_2O) = 1.690$ eV to $E_{em}(+3H_2O) = 1.783$ eV. Again, it was important to take into account explicit H-bonding in order to predict the correct order and reasonable relative excitation and emission energies of the solute molecule in different solvents.

The predicted and observed absorption (solid line with circles) and emission (dotted line with diamonds) energies in different solvents are also compared in Figure 5. Except for the absorption energy in $C_2H_4Cl_2$ (point a), the relative absorption and emission energies of this molecule in acetone, acetonitrile, MeOH, and water (including explicit H-bonding solvent molecules) are predicted in the correct order and with proportional solvent shifts compared with experimentally determined values, although the experimental solvent shifts are larger.

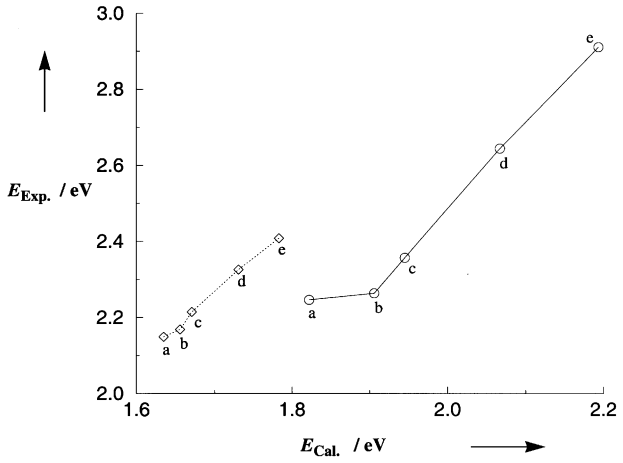

Figure 5. Correlation between the calculated and observed absorption (—— with○) and emission (•••• with ◇) energies for Abdel-Halim's merocyanine in a) $C_2H_4Cl_2$, b) acetone, c) acetonitrile, d) $+2CH_3OH$ in MeOH, and e) $+3H_2O$ in water. The figure is generated using Xmgr.[40]

The dipole moment of Abdel-Halim's merocyanine also increased with solvent polarity, and further increased when explicit H bonds with CH_3OH or H_2O were included. In all solutions (including gas phase), the solute dipole moment decreases during the $S_0 \rightarrow S_1$ transition. As explained by Reichardt,[1] the Franck–Condon S_1 state is in a strained solvent cage of oriented dipoles which are not correctly disposed to efficiently stabilize the S_1 state. Thus, with increasing solvent polarity, the energy of the S_0 state is lowered more than that of the excited state, therefore the excitation energy increases, and this produces the blue shift. After relaxation of both the solute and solvent molecules, the solute dipole moment further decreases in the relaxed S_1 state, then increases in the $S_1 \rightarrow S_0$ process. Again with increasing solvent polarity, the emission energy increases, and a blue shift is observed in the emission process since the energy of the Franck–Condon S_0 state is lowered more than that of the relaxed S_1 state.

The main bond lengths of Abdel-Halim's merocyanine in gas phase and in H_2O solution (with and without explicit H-bonding H_2O molecules), for both the relaxed S_0 and S_1 states, are given in Figure 3. The corresponding molecular orbital plots for the electron in the HOMO (S_0 state) or the promoted electron in the S_1 state are given in Figure 6. The plots for the $+3H_2O$ model are

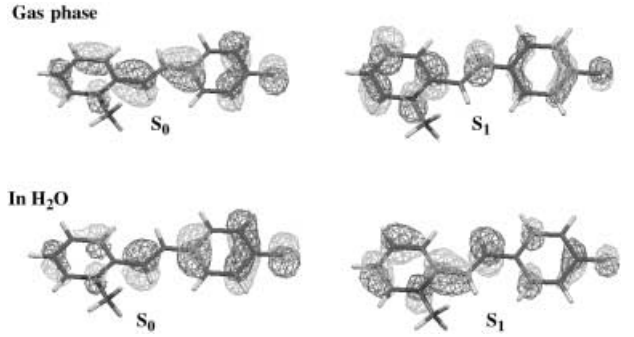

Figure 6. Molecular orbital plots for the electron in HOMO of the S_0 state and the $\pi \rightarrow \pi^*$ promoted electron in the S_1 state Abdel-Halim's merocyanine in gas phase and in H_2O solution.

similar to the corresponding ones without H-bonding H_2O molecules, and therefore are not presented here.

The three central C–C bonds in the gas-phase S_0 state structure are of nearly equal bond lengths, with C_2–C_3 slightly longer than C_1–C_2 and C_3–C_4. In solvent, however, the C_2–C_3 bond gradually becomes shorter than the C_1–C_2 and C_3–C_4, and the bond length of C_7–O_8 increases with increasing solvent polarity. The structure reaches another extreme in H_2O solution, and becomes even more polarized when adding three explicit H-bonding H_2O molecules. The bond lengths of C_1–C_2, C_2–C_3, C_3–C_4 and C_7–O_8 change from (1.433, 1.378, 1.433, and 1.304 Å), to (1.438, 1.370, 1.439, and 1.325 Å), respectively, after adding the three H_2O molecules. From S_0 to the relaxed S_1 state, in gas phase the bond lengths of C_1–C_2, C_3–C_4 and C_7–O_8 are increased, and C_2–C_3 is shortened. By contrast, in solution, the lengths of C_1–C_2, C_3–C_4 and C_7–O_8 are decreased, and C_2–C_3 is increased. When adding three H-bonding H_2O molecules, C_2–C_3 (1.414 Å) becomes the longest, and C_1–C_2 (1.410 Å) and C_3–C_4 (1.418 Å) are shortest among all the S_1 state structures in different solutions.

Unlike the case for the S-TBA, both the excitation and emission energies of the Abdel-Halim's merocyanine in gas phase are lower than the ones in solvents. The reason is that the HOMOs of this molecule in the S_0 state are all occupied by the atomic π orbitals, with different contributions in different cases. In solution, the S_0 state solute is more polarized, with electronic densities shifting toward the right side of the molecule. All absorption of $S_0 \rightarrow S_1$ processes are $\pi \rightarrow \pi^*$ electronic transitions. During excitation, the electronic densities shift leftward relative to the S_0 state, and thus the dipole moment decreases. Intermolecular charge transfer also occurred through H-bonding interactions. The ESP charge of atom O_8 of the S_0 state solute in H_2O solution was -0.802. It decreased to -0.320 in the $+3H_2O$ model, since the three oxygens in the H-bonding H_2O molecules were now the main electron accepting atoms with very negative ESP charges of -0.919, -0.919 and -0.922. The dipole moment of the quantum region was then increased after adding the explicit H-bonding solvent molecules.

All emission $S_1 \rightarrow S_0$ processes are $\pi^* \rightarrow \pi$ electronic transitions. The LUMO and HOMO energy gap increases with increasing solvent polarity (including gas phase), and therefore, blue shifts were found for both the absorption and emission processes.

3.3. The Rigid Aminocoumarin C153

The calculated and experimentally observed[1, 11] vertical excitation (E_{abs}) and emission (E_{em}) energies of the rigid aminocoumarin C153 (see structures in Figure 7) are given in Table 4. A red shift has been observed with increasing solvent polarity for both the absorption and emission bands, that is $E_{abs(em)}$(cyclohexane) > $E_{abs(em)}$(ethyl acetate) > $E_{abs(em)}$(acetonitrile) > $E_{abs(em)}$(ethanol) > $E_{abs(em)}$(H_2O). Our calculations correctly predicted this order except for the absorption and emission energies in acetonitrile and in ethanol. The dielectric constant of acetonitrile ($\varepsilon = 37.5$) is much larger than that of ethanol ($\varepsilon = 24.3$). Therefore, without considering explicit interactions between the solute and solvent molecules, we predicted the $E_{abs(em)}$(acetonitrile) were closer to $E_{abs(em)}$(H_2O), and smaller than the $E_{abs(em)}$(ethanol) values. The reason that experimentally $E_{abs(em)}$(acetonitrile) > $E_{abs(em)}$(ethanol) should again be caused by the solute structure becoming more polarized in ethanol through explicit H-bonding interactions with ethanol (C_2H_5OH) molecules. Very recently, IR spectra of C153 in solvent mixtures containing methanol confirm the formation of a hydrogen bond between methanol and C153.[15] We therefore added one C_2H_5OH H bond to atom O_{16} (see Figure 8a) and geometry optimized the structures in both the S_0 and S_1 state using the COSMO model. The SCRF/VSCRF calculations then show that the E_{abs}(+1C_2H_5OH) and E_{em}(+1C_2H_5OH) lie

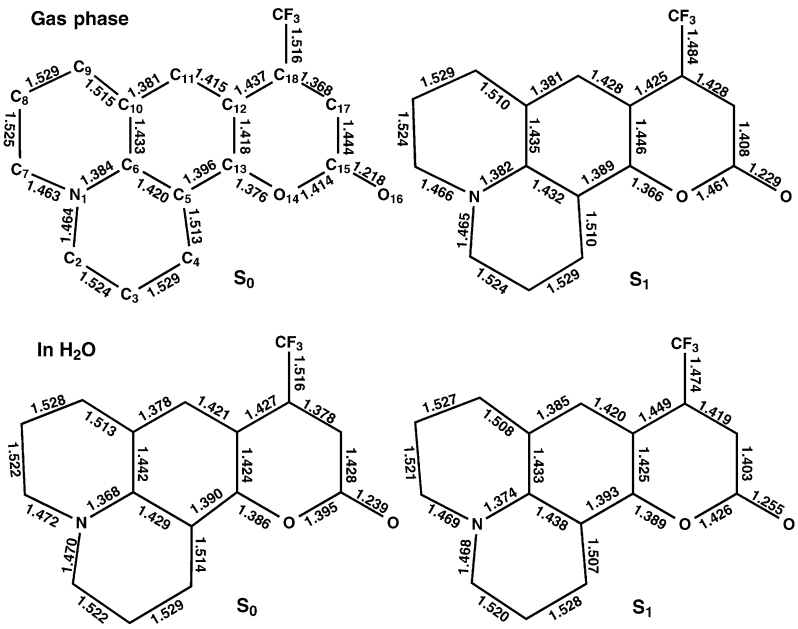

Figure 7. The main bond lengths of the rigid aminocoumarin C153 in gas phase and in H_2O (without explicit H_2O molecules) solution for both the relaxed S_0 and S_1 state.

Table 4. *SCRF/VSCRF calculated and experimentally observed absorption (E_{abs}) and emission (E_{em}) energies (eV), and the S_0 (μ_{S0}) and S_1 (μ_{S1}) state dipole moment values (D) for the rigid aminocoumarin C153 in different solvents.*

	Absorption				Emission			
			E_{abs}				E_{em}	
Solvent	μ_{S0}[a]	μ^{v}_{S1}[b]	Calculation	Experiment	μ_{S1}[c]	μ^{v}_{S0}[d]	Calculation	Experiment
Gas phase	8.50	12.71	2.564		12.78	9.23	2.223	
Cyclohexane	10.48	16.13	2.409	3.155	16.26	11.33	2.094	2.725
Ethyl acetate	12.70	18.54	2.273	3.032	20.37	15.03	1.876	2.475
Acetonitrile	14.49	20.16	2.176	2.966	23.06	17.75	1.720	2.380
Ethanol {no H-bonding	14.30	19.97	2.186	2.945	22.74	17.45	1.739	2.335
Ethanol {$+1C_2H_5OH$	16.30	22.25	2.155		25.02	19.44	1.711	
H_2O {no H-bonding	14.83	20.57	2.155	2.884	23.80	18.56	1.680	2.259
H_2O {$+2H_2O$	16.21	21.87	2.072		24.99	19.96	1.644	

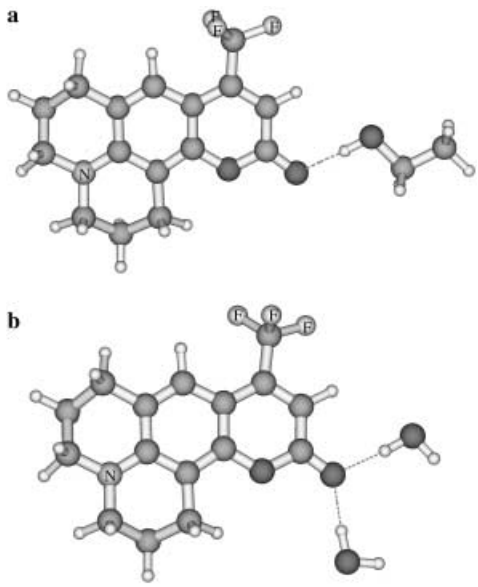

Figure 8. Explicit H-bonding structures of a) $+1C_2H_5OH$ and b) $+2H_2O$ models for the rigid aminocoumarin C153 in ethanol and in water solutions, respectively.

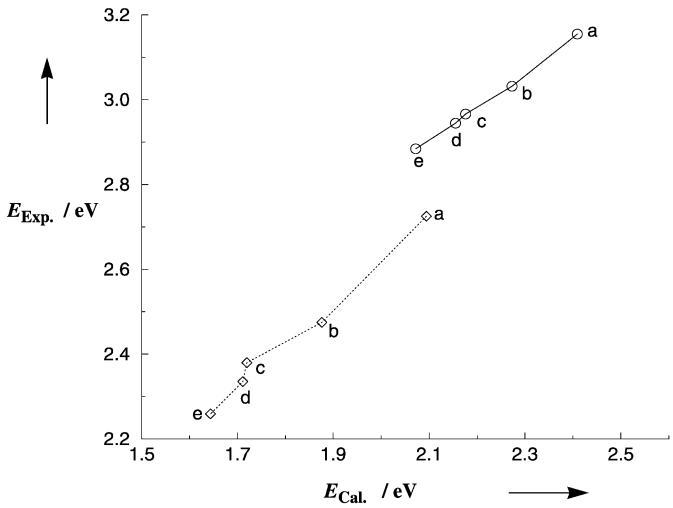

Figure 9. Correlation between the calculated and observed absorption (—— with ○) and emission (•••• with ◇) energies for aminocoumarin C153 in a) cyclohexane, b) ethyl acetate, c) acetonitrile, d) $+1C_2H_5OH$ in ethanol, and e) $+2H_2O$ in water.

lower by 0.031 and 0.028 eV, respectively, than the calculated energies without explicit solvent, so $E_{abs(em)}$(acetonitrile) > $E_{abs(em)}$(ethanol) is achieved.

Similar to the calculations of Abdel-Halim's merocyanine in H_2O solution, we added two H_2O molecules around atom O_{16} (see Figure 8 b) to see if we could improve the relative values between the $E_{abs(em)}(H_2O)$ and the $E_{abs(em)}$ energies in other solutions. This lowered the $E_{abs}(H_2O)$ and $E_{em}(H_2O)$ from 2.155 and 1.680 eV to 2.072 and 1.644 eV, respectively. Except for the energies $E_{abs}(+2H_2O) - E_{abs}$(cyclohexane) and $E_{abs}(+2H_2O) - E_{abs}$(ethyl acetate) being larger with a slightly greater deviation from experiment, all other relative energies between $E_{abs(em)}(+2H_2O)$ and the $E_{abs(em)}$ values in other solutions were increased to be closer to the observed data when explicit waters are included.

The predicted and observed absorption (solid line with circles) and emission (dotted line with diamonds) energies in different solvents are also compared in Figure 9. As expected, the absolute values of the predicted energies were lower than the observed ones. However, the relative energies in general are predicted very well.

The main bond lengths of C153 in the gas phase and in H_2O solution for both the relaxed S_0 and S_1 states are given in Figure 7. The corresponding molecular orbital plots for the electron in the HOMO (S_0 state) or the promoted electron in the S_1 state are given in Figure 10. Unlike the extended molecules of S-TBA and Abdel-Halim's merocyanine, the electronic structures of the S_0 state C153 look very similar in the gas phase and solutions. Though C153 is rigidified, its conformation still changes with solvent polarity. The largest change in the geometry upon solvation is the distance of C_{15}–O_{16}, from 1.218 Å in the gas phase to 1.239 Å in H_2O, and to 1.253 Å when adding two explicit H-bonding H_2O molecules. Meanwhile the bond lengths of N_1–C_6, C_{10}–C_{11}, C_5–C_{13}, C_{12}–C_{18}, O_{14}–C_{15} and C_{15}–C_{17} decrease with increasing solvent polarity. Other bond lengths in the aromatic rings are increased accordingly. In the relaxed S_1 state, the solute geometry also changes with solvent polarity. Unlike the S_0 state, the distance of C_{18}–CF_3 in the relaxed S_1 state also varies with solvent.

It is very well known for this molecule that intramolecular charge transfer occurs during the $S_0 \rightarrow S_1$ and $S_1 \rightarrow S_0$ processes,[1]

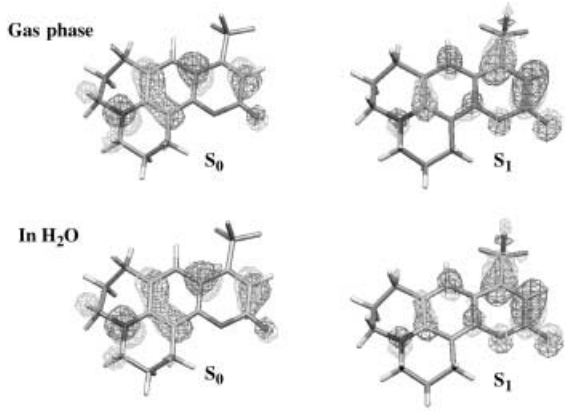

Figure 10. *Molecular orbital plots for the electron in HOMO of the S_0 state and the $\pi \rightarrow \pi^*$ promoted electron in the S_1 state C153 in gas phase and in H_2O solution.*

which corresponds to the increasing (during the absorption) and decreasing (during the emission) of the dipole moment. As shown in the molecular orbital plots of Figure 10, during the $S_0 \rightarrow S_1$ electronic transition, the electron in the HOMO shifted from the left side of the molecule to the right. Further, intramolecular charge transfer increases with increasing solvent polarity. This explains the significant red shifts of the absorption and emission bands for this molecule with increasing solvent polarity. The charge-shifting upon excitation from electron donating N-side to electron accepting O-side is also shown from the stronger H-bonding interactions of the relaxed S_1 state C153 in water. The two H-bond (H···O) distances (in model Figure 8b) are decreased from 1.780 and 1.805 Å in the S_0 state to 1.742 and 1.754 Å in the relaxed S_1 state.

3.4. Nile Red

The predicted and observed[16, 17] vertical excitation (E_{abs}) and emission (E_{em}) energies of Nile red (see structures in Figure 11) are given in Table 5. Similar to the dye C153, a red shift has been found for both the absorption and emission bands for Nile red in solutions with increasing solvent polarity, and our calculations also predicted the same excitation and emission energy ordering of $E_{abs(em)}$(cyclohexane) > $E_{abs(em)}$(acetone) > $E_{abs(em)}$(DMF) > $E_{abs(em)}$(MeOH) > $E_{abs(em)}$(H_2O). Here, even without including the explicit H-bonding interactions, we predicted the correct order of $E_{abs(em)}$(DMF) > $E_{abs(em)}$(MeOH), although the dielectric constant of DMF ($\varepsilon = 36.7$) is larger than that of MeOH ($\varepsilon = 32.6$). It may because the DMF and MeOH molecules have different radii ($r = 3.7$ Å for DMF *versus* $r = 2.5$ Å for MeOH) which were used in all the COSMO, SCRF and VSCRF calculations. This parameter defines the boundary between the solute and the solvent region by rolling a probe sphere with the radius r around the solute van der Waals surface. When the solvent dielectric constants are close to each other, the different solvent radii

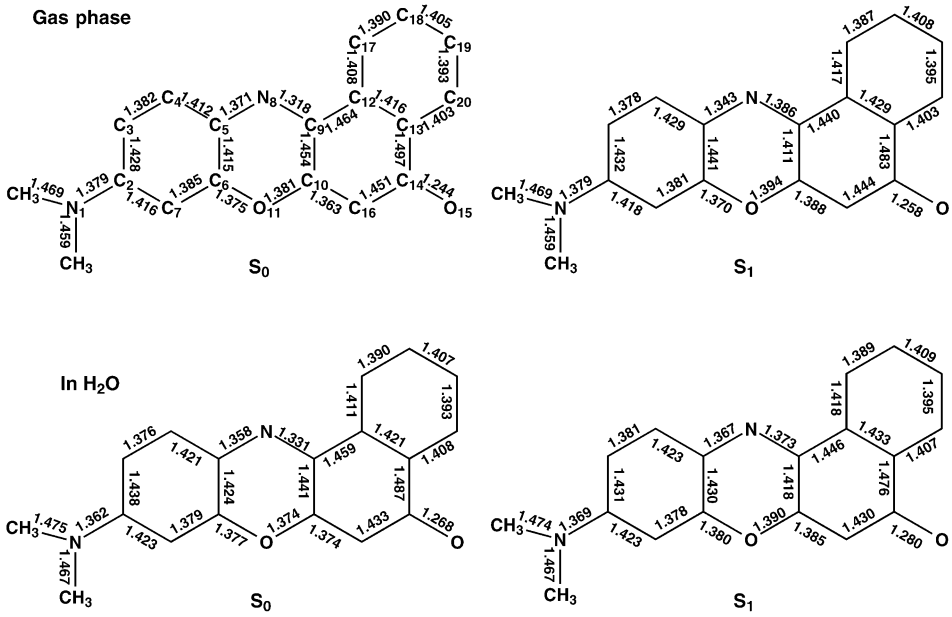

Figure 11. *The main bond lengths of Nile red in gas phase and in H_2O solution for both the relaxed S_0 and S_1 state.*

Table 5. *SCRF/VSCRF calculated and experimentally observed absorption (E_{abs}) and emission (E_{em}) energies (eV), and the S_0 (μ_{S0}) and S_1 (μ_{S1}) state dipole moment values (D) for Nile red in different solvents.*

		Absorption				Emission			
				E_{abs}				E_{em}	
Solvent		μ_{S0}[a]	μ^{v}_{S1}[b]	Calculation	Experiment	μ_{S1}[c]	μ^{v}_{S0}[d]	Calculation	Experiment
Gas phase		9.62	12.44	1.935		12.04	10.57	1.610	
Cyclohexane		12.23	16.28	1.804	2.417	15.44	13.44	1.548	
Acetone		17.86	21.82	1.600	2.326	22.46	20.44	1.413	2.016
DMF		18.28	22.21	1.587	2.292	22.90	20.88	1.405	1.984
MeOH	no H-bonding	18.81	22.31	1.581	2.255	23.24	21.00	1.399	1.931
	$+1CH_3OH$	18.60	21.88	1.557		22.72	21.34	1.391	
H_2O	no H-bonding	19.46	23.06	1.560		23.33	21.69	1.391	1.865
	$+2H_2O$	21.37	23.65	1.525		25.29	23.81	1.353	

can make a difference in the solvation and hence the excitation and emission energies. Notice, however, that the predicted difference is very small, and much less than the experimental difference.

To further improve the relative energies, we included explicit H bonds to atom O_{15}, one CH_3OH molecule (see Figure 12a) and

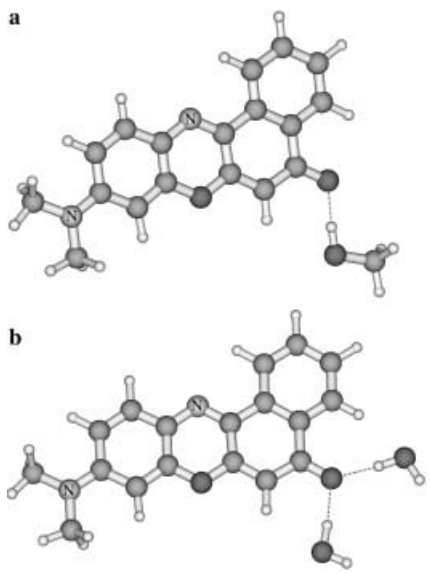

Figure 12. Explicit H-bonding structures of a) + 1CH_3OH and b) + 2H_2O models for Nile red in MeOH and in water solutions, respectively.

two H_2O molecules (Figure 12b) in MeOH and in H_2O, respectively. This increased all the relative energies between $E_{abs(em)}(+2H_2O)$ and $E_{abs(em)}(+1CH_3OH)$ and the $E_{abs(em)}$ values for Nile red in other solutions bring them much closer to the corresponding experimental data.

Again, similar to the molecule C153, the dipole moment of Nile red increases during the absorption and decreases in the emission process, consistent with the red shift of the absorption and emission bands with increasing solvent polarity.

The main bond lengths of the Nile red in the gas phase and in H_2O for both the relaxed S_0 and S_1 states are given in Figure 11. The corresponding molecular orbital plots for the electron in the HOMO (S_0 state) or the promoted electron in the S_1 state are given in Figure 13. The HOMOs of the S_0 state of Nile red in the gas phase and in different solvents are all occupied by atomic π orbitals. The contributions of the atomic π orbitals to the HOMO varied with solvent and were modified by explicit H-bonding interactions. The ESP charge of O_{15} changed from -0.631 to -0.388 after adding the two H_2O molecules, since the negative charge transfers to the oxygen atoms (with ESP charges of -0.903 and -0.894) of the water molecules. In the ground state upon solvation and with increasing solvent polarity, there is an increase in the bond lengths of C_{14}–O_{15}, C_{10}–C_{16}, C_{12}–C_{13}, N_8–C_9, C_4–C_5, and C_2–C_3, and a decrease in N_1–C_2, C_3–C_4, C_5–N_8, C_9–C_{12}, C_{10}–O_{11}, C_{13}–C_{14}, and C_{14}–C_{16}. During the $S_0 \rightarrow S_1$ electronic transition, the distance of N_8–C_9 is significantly

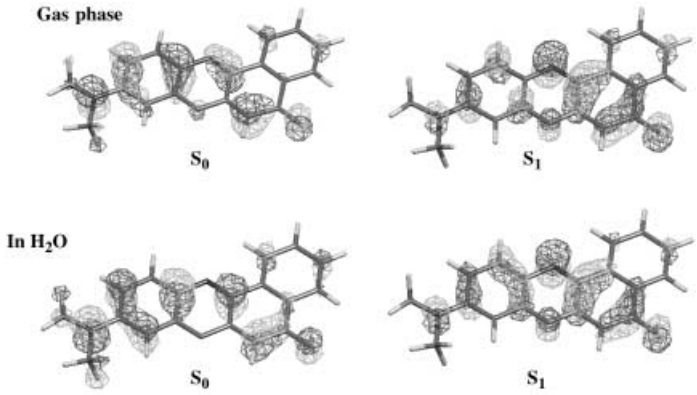

Figure 13. Molecular orbital plots for the electron in HOMO of the S_0 state and the $\pi \rightarrow \pi^*$ promoted electron in the S_1 state Nile red in gas phase and in H_2O solution.

increased in all cases, with the intramolecular charge transfer from N_1 to N_8. The charge transfer during the $\pi \rightarrow \pi^*$ and also $\pi^* \rightarrow \pi$ processes result in variation of the solute dipole moment and thus produce the solvatochromic shifts of the absorption and emission bands of Nile red in solution.

4. Conclusion

Herein, we used the SCRF/VSCRF method plus the COSMO solvation model to correctly predict the solvatochromic shifts of both the absorption and emission bands for four dye molecules, S-TBA merocyanine, Abdel-Halim's merocyanine, the rigid aminocoumarin C153, and Nile red. We found that H-bonding solvent interactions were important to include in calculations to predict the correct order of the excitation and emission energies.

For the relaxed S_0 or S_1 state of the solute molecule, we see that intramolecular charge transfer occurs upon solvation, and will increase with increasing solvent polarity. Intermolecular charge transfer will also occur through explicit H-bonding interactions. In solvents of differing polarity, there will be different electronic structures for the solute, resulting in different molecular structures. The intramolecular and intermolecular charge transfer will occur during $\pi \rightarrow \pi^*$ and $\pi^* \rightarrow \pi$ electronic transitions, causing an increase or decrease in the solute dipole moment. All these factors work together to produce predictable solvatochromic shifts in absorption and emission.

Acknowledgements

We thank Novartis and the NIH (GM43278 and GM39914 for LN, WGH, and TL, GM57464 and AG15430 for KH, and GM45607 for DB) for financial support. F. Himo would like to thank the Wenner–Gren Foundations for financial support while at The Scripps Research Institute, and A. Toutchkine thanks the Leukemia and Lymphoma Society. We also thank one of the reviewers who pointed out a structural error in the original manuscript.

Supporting Information Available: A long version of Table 2 which contains more geometric parameters for S-TBA in the gas phase, in C_6H_6 and in MeOH solutions, and the detailed descriptions for Figures 6, 10, and 13 are available at http://www.chemphyschem.org.

Keywords: density functional calculations · self-consistent reaction field · solvatochromism · solvent-sensitive dyes · vertical excitation

[1] C. Reichardt, *Solvent Effects in Organic Chemistry*, Verlag Chemie, Weinheim, **1979**.
[2] N. J. Turro, *Modern Molecular Photochemistry* University Science Books, Mill Valley, **1991**.
[3] T. Liu, W.-G. Han, F. Himo, G. M. Ullmann, D. Bashford, A. Toutchkine, K. Hahn, L. Noodleman, unpublished results.
[4] M. J. Thompson, T. Liu, D. Bashford, E. D. Getzoff, L. Noodleman, unpublished results.
[5] J. Chen, L. Noodleman, D. A. Case, D. Bashford, *J. Phys. Chem.* **1994**, *98*, 11 059 – 11 068.
[6] D. Bashford, *Scientific Computing in Object Oriented Parallel Environments (Lecture Nodes in Computer Science)*; Springer: Berlin, **1997**, 240.
[7] J. Li, C. L. Fisher, J. L. Chen, D. Bashford, L. Noodleman, *Inorg. Chem.* **1996**, *35*, 4694 – 4702.
[8] J. Li, M. R. Nelson, C. Y. Peng, D. Bashford, L. Noodleman, *J. Phys. Chem. A* **1998**, *102*, 6311 – 6324.
[9] K. M. Hahn, A. S. Waggoner, D. L. Taylor, *J. Biol. Chem.* **1990**, *265*, 20 335 – 20 345.
[10] S. T. Abdel-Halim, *J. Chem. Soc. Faraday Trans.* **1993**, *89*, 55 – 57.
[11] G. Jones II, W. R. Jackson, C. Choi, W. R. Bergmark, *J. Phys. Chem.* **1985**, *89*, 294 – 300.
[12] T. Gustavsson, L. Cassara, V. Gulbinas, G. Gurzadyan, J.-C. Mialocq, S. Pommeret, M. Sorgius, P. van der Meulen, *J. Phys. Chem. A* **1998**, *102*, 4229 – 4245.
[13] P. K. McCarthy, G. J. Blanchard, *J. Phys. Chem.* **1993**, *97*, 12 205 – 12 209.
[14] A. Mühlpfordt, R. Schanz, N. P. Ernsting, V. Farztdinov, S. Grimme, *Phys. Chem. Chem. Phys.* **1999**, *1*, 3209 – 3218.
[15] R. Królicki, W. Jarzeba, M. Mostafavi, I. Lampre, *J. Phys. Chem. A* **2002**, *106*, 1708 – 1713.
[16] M. M. Davis, H. B. Hetzer, *Anal. Chem.* **1966**, *38*, 451 – 461.
[17] D. L. Sackett, J. Wolff, *Anal. Biochem.* **1987**, *167*, 228 – 234.
[18] A. Toutchkine, V. Kraynov, K. Hahn, *J. Am. Chem. Soc.* **2003**, *125*, 4132 – 4145.
[19] ADF2000.02, Scientific Computing & Modeling, Amsterdam, **2000**.
[20] G. Te Velde, F. M. Bickelhaupt, E. J. Baerends, C. F. Guerra, S. J. A. Van Gisbergen, J. G. Snijders, T. Ziegler, *J. Comput. Chem.* **2001**, *22*, 931 – 967.
[21] S. H. Vosko, L. Wilk, M. Nusair, *Can. J. Phys.* **1980**, *58*, 1200 – 1211.
[22] A. D. Becke, *Phys. Rev. A* **1988**, *38*, 3098.
[23] J. P. Perdew, *Phys. Rev. B* **1986**, *33*, 8822; **1986**, *34*, 7406 (erratum).
[24] A. Klamt, G. Schuurmann, *J. Chem. Soc., Perkin Trans.* **1993**, *2*, 799 – 805.
[25] A. Klamt, *J. Phy. Chem.* **1995**, *99*, 2224 – 2235.
[26] A. Klamt, V. Jones, *J. Chem. Phys.* **1996**, *105*, 9972 – 9981.
[27] D. Bashford, *Curr. Opin. Struct. Biol.* **1991**, *1*, 175.
[28] D. Bashford, K. Gerwert, *J. Mol. Biol.* 1992, *224*, 473 – 486.
[29] C. Lim, D. Bashford, M. Karplus, *J. Phys. Chem.* **1991**, *95*, 5610 – 5620.
[30] D. Bashford, D. A. Case, C. Dalvit, L. Tennant, P. E. Wright, *Biochemistry* **1993**, *32*, 8045 – 8056.
[31] T. Ziegler, A. Rauk, E. J. Baerends, *Theor. Chim. Acta* **1977**, *43*, 261 – 271.
[32] T. Ziegler, *Chem. Rev.* **1991**, *91*, 651 – 667.
[33] K. Hahn, R. DeBiasio, D. L. Taylor, *Nature* **1992**, *359*, 736 – 738.
[34] W.-G. Han, T. Lovell, T. Liu, L. Noodleman, *ChemPhysChem* **2002**, *3*, 167 – 178.
[35] A. Klamt, *J. Phys. Chem.* **1996**, *100*, 3349 – 3353.
[36] A. Mishra, R. A. Behera, P. K. Behera, B. K. Mishra, G. B. Behera, *Chem. Rev.* **2000**, *100*, 1973 – 2011.
[37] P. Flükiger, H. P. Lüthi, S. Portmann, J. Weber, *MOLEKEL 4.0* Swiss Center for Scientific Computing, Manno, Switzerland, **2000**.
[38] XMOL 1.3.1 Copyright 1990, 1991, 1992, 1993 Research Equipment, Inc. d/b/a Minnesota Supercomputer Center, Inc.
[39] T. Sato, B. V. Smith, *XFIG Drawing Program for X Window System* Copyright (c) 1997 – 2000.
[40] Xmgr V.4.1.2. Copyright 1991 – 1995 Paul J. Turner. Copyright 1996 – 1998 ACE/gr Development Team.

Received: April 22, 2003 [F 801]

